Vibration of an aircraft model

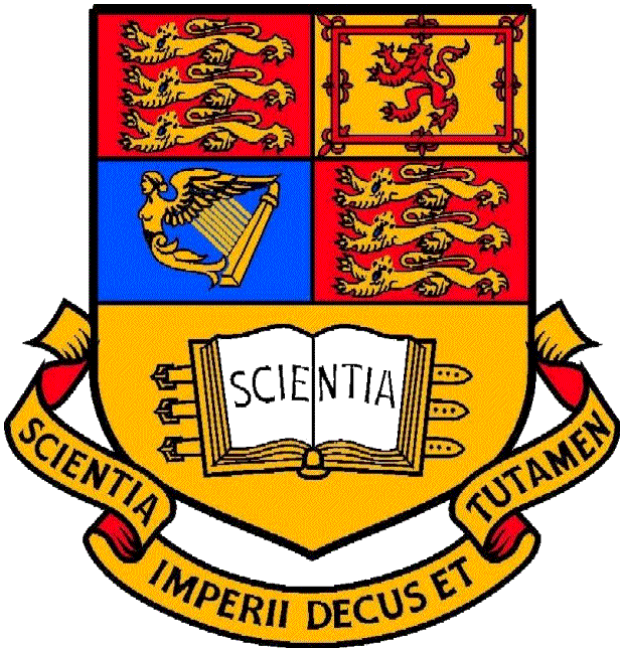

Xerxes Chong Xian

CID: 01389744

Submission Date: 3 December 2018

Abstract

This experiment explores the dynamic response of an aircraft by vibrating a model aircraft. The model was tested at multiple frequencies of vibration and an experimental resonant frequency of 17.30 Hz and damping ratio of 0.00631 was found. Vibrating the model at the experimental resonant frequency and performing eigenvector analysis showed the dominance of wing deflection in the model aircraft's first modal shape. Plots of acceleration, velocity and displacement against frequency illustrate the effect of resonance on these quantities. The Nyquist plots confirm the effect of dampening on the accuracy of results.

Table of Contents

List of Figures

List of Tables

Chapter 1

1 Introduction

1.1 Introduction

An aircraft in flight sustains a variety of dynamic loadings. Vibrations from the engines and fluctuating loads on the wing are a discomforting experience for those onboard. At high wind speeds, the interaction of aerodynamics, structure stiffness and inertial forces can result in fluttering of lifting and control surfaces due to aeroelasticity (1). This deformation of the structure leads to a loss of structural integrity and control, proving disastrous if at resonant frequency. This can occur especially if the aircraft was not designed with enough damping. An understanding of the aircraft's response to dynamic loading, especially the deformations at its normal modes (2), are paramount for the comfort and safety of its operation.

In this experiment, a simplified model of an aircraft is tested. The model is vibrated by vibrators and data is gathered from accelerometers attached. Eigenvalue analysis is performed to obtain the natural undamped frequency, damping ratio and to determine the first mode shape.

1.2 Objectives

To explore the dynamic response of the model aircraft for its first mode, by determining the:

1. first undamped natural frequency by interpretation of the graphs of:
    a. Magnitudes of displacement, velocity and acceleration against the frequency of vibration as well as the Nyquist plots, which plot the in and out-of-phase components of the response.
    b. Phases of displacement, velocity and acceleration against the frequency of vibration
2. damping ratio.
3. first mode shape.

Chapter 2

2 Experimental Apparatus and Procedure

A detailed explanation of the apparatus used, procedure and underlying theories implemented in this experiment can be found in the laboratory handout (3). A brief summary of it is presented in this report.

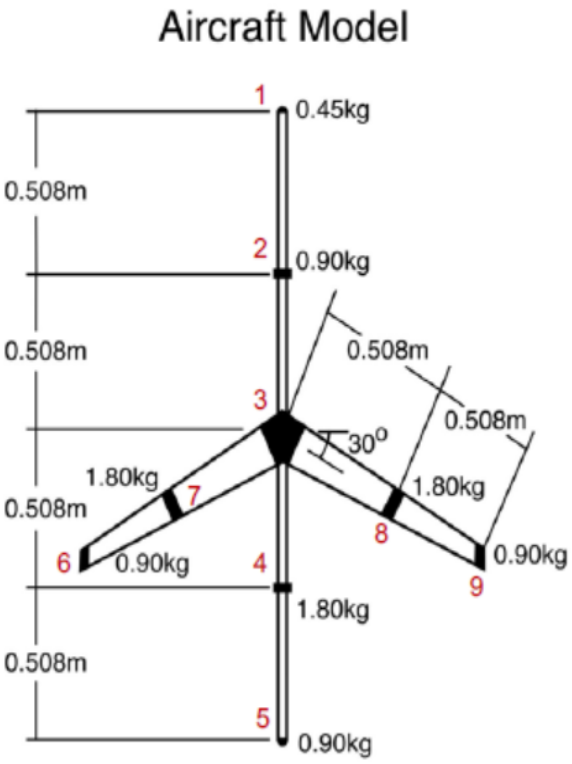

Figure 2.1 Schematic of the model aircraft

Figure 2.2 Picture of the model aircraft in the tripod frame

2.1 Experimental Apparatus

Figure 2.1 shows the schematic layout of the model aircraft. Concentrated masses are used to represent the mass distributions on an aircraft. The locations of all 9 accelerometers are numbered in red.

The model is suspended freely from a tripod frame as shown in Figure 2.2. A uniform circular cylinder and 2 tapered rectangular bars form the fuselage and wings respectively and it is assumed to the symmetric along the fuselage. 9 concentrated masses are attached on various parts of the model along with 9 accelerometers. Goodman vibrators are connected to the wings at mid-span. The structure is excited by the vibrators and the outputs of the accelerometers are passed to a data acquisition system. This data is processed to obtain the amplitude and phase of the model's response.

2.2 Experimental Procedure

Objectives 1 and 2 were achieved by testing the model at varying frequencies of vibration. The data from a single accelerometer (Number 9) was processed and filtered using the Measure Foundry Software provided and the amplitudes and phase angles of the model's response was

obtained. After processing via the Microsoft Excel spreadsheet provided, the undamped natural frequency and damping ratio was found.

For Objective 3, the model was vibrated at the undamped natural frequency found and the data from all accelerometers were collected and processed. As not all accelerometers were mounted on the same side, calibration factors were applied as needed to the amplitudes and phase angles. Eigenvalues analysis was performed, following which the eigenvectors and coordinates obtained from the spreadsheet were plotted to illustrate the first mode shape.

Chapter 3

3 Experimental Results

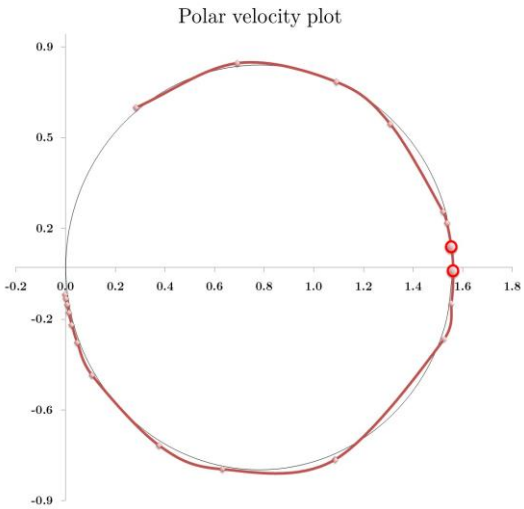

Figure 3.1 The 2 highlighted data points closest to the x-axis were used to calculate the undamped natural frequency and damping ratio. The quality of fit was 97.9%

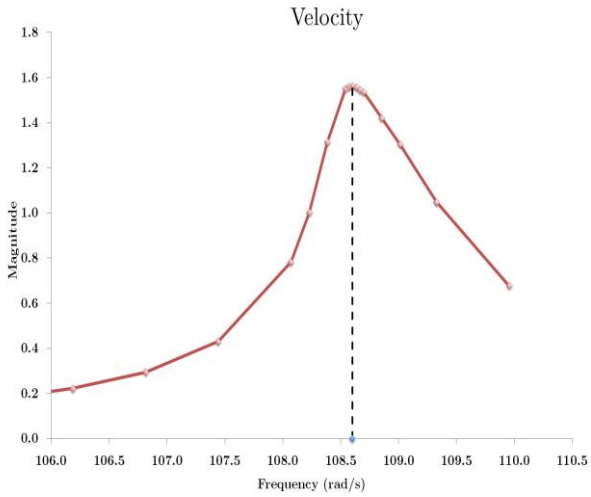

Figure 3.2 The black dotted line represents the experimental resonance frequency that corresponds to the peak velocity magnitude

Unprocessed data can be found in Appendix A. The accelerations, velocities, displacement and phase angles of the response to the different applied frequencies were plotted against the applied frequencies. However, for the purpose of this section, only the plot of magnitude of velocity against frequency is shown. Only the Nyquist plot for the velocity response is shown. The variables for the in and out-of-phase components makes approximating them as circles possible (4). The fitting circle represented by the solid black lines was also plotted. The remaining frequency graphs and Nyquist plots for acceleration and displacement can be found in Appendix B.

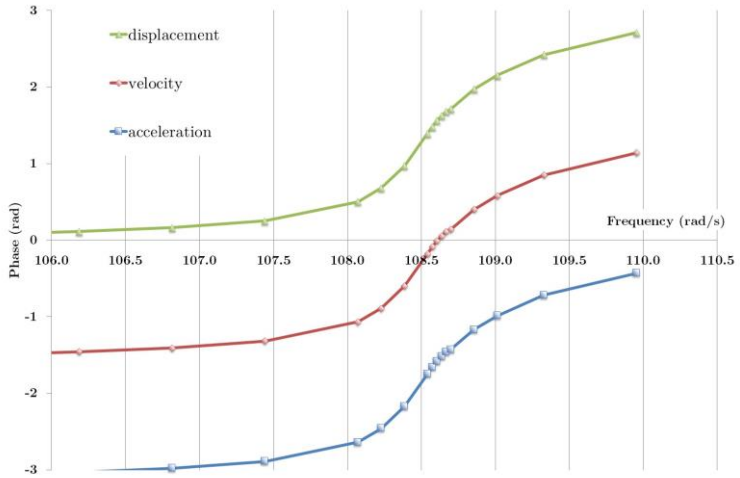

Figure 3.3 Plot of phase vs frequency. The x-intercept of the velocity plot corresponds to the resonant frequency

From Figure 3.3, there are 19 points within $\pm\frac{\pi}{2}$ of the resonant frequency.

3.1 Obtaining the undamped natural frequency and the damping ratio

The equation for the undamped natural frequency, ω_u is defined as:

$$\omega_u^2 = \frac{\omega_A^2 \omega_B \tan\theta_{\dot{r}_B} - \omega_B^2 \omega_A \tan\theta_{\dot{r}_A}}{\omega_B \tan\theta_{\dot{r}_B} - \omega_A \tan\theta_{\dot{r}_A}}$$

Where ω_A, ω_B, $\theta_{\dot{r}_A}$ and $\theta_{\dot{r}_B}$are the frequencies and velocity phase angles at any 2 data points. While any 2 data points can be selected to calculate the undamped natural frequency, points were selected based on their proximity to the experimental natural frequency. Picking points close to the natural frequency reduces the effects of the resonant modes of the system (3). This is performed by selecting the pairs of points that lie closest to the x-axis of Figure 3.1 as these points are the most in-phase with the model's response.

To obtain the damping ratio, the follow equations were used.

$$\frac{c}{m} = \frac{\omega_B^2 - \omega_A^2}{\omega_B \tan\theta_{\dot{r}_B} - \omega_A \tan\theta_{\dot{r}_A}} = 2\alpha$$

$$\xi = \frac{\alpha}{\omega_u}$$

Rearranging to obtain α, the damping ratio ξ, is obtained by dividing α by ω_u. To increase accuracy, 5 pairs of data points were chosen to obtain 10 possible values of ω_u and ξ. These points are highlighted in bold and red in Appendix A. The average was obtained and displayed in Table 3.1. This is similar to the frequency found from reading the frequency corresponding to peak velocity magnitude in Figure 3.2 and the x-intercept of the velocity plot in Figure 3.3.

Table 3.1 Average undamped natural frequency and damping ratio

Averaged Undamped Natural Frequency, ω_u	Average damping ratio, ξ
17.30 Hz / 108.70 rad/s	0.00631

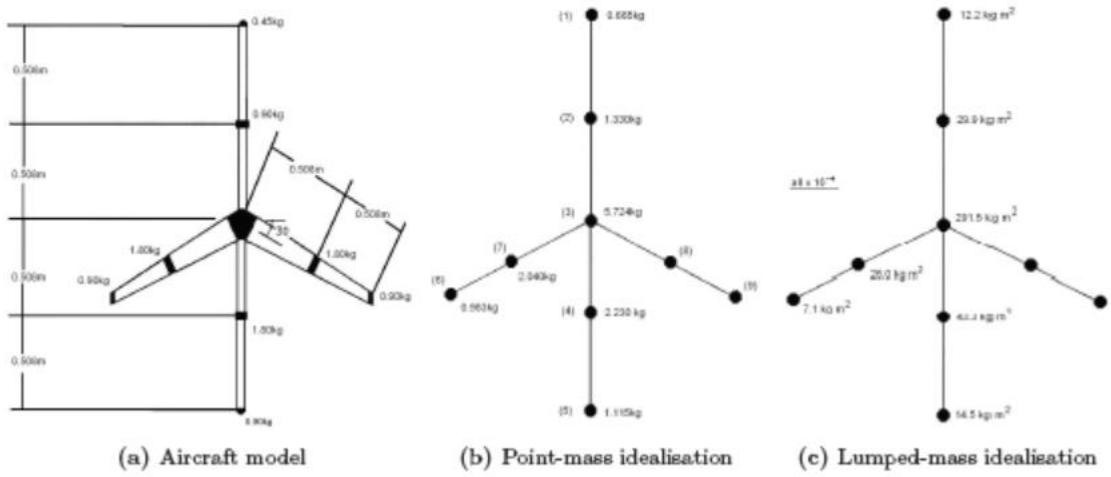

Figure 3.4 The schematic of the point-mass and lumped-mass idealisation is compared with the model aircraft

The experimental values obtain for undamped natural frequency is now compared to those obtain by using a point-mass and lumped mass idealisation of the model aircraft (3). The schematic of the 2 theoretical idealisations are compared with the model in Figure 3.4.

Table 3.2 Comparison of experimental and theoretical undamped natural frequency

Source	Frequency (Hz)
Point-mass model	15.65
Lumped-mass model	15.69
Experimental	17.30

From Table 3.2, the experimental undamped natural frequency deviates from the idealised result. The point-mass model and lumped-mass model deviate by 9.5% and 9.3% respectively, from the experimental data.

3.2 Obtaining the first mode shape

The model aircraft was vibrated at 17.30 Hz and data from all 9 accelerometers were collected and calibrated in the Microsoft Excel spreadsheet. The numerical simulation performs an eigenvalue analysis of the point-mass idealised model of the aircraft to obtain the numerical eigenvalues and eigenvectors. The plots of eigenvectors and coordinates for the first mode of the wing and fuselage are shown in *Figure 3.5* and *Figure 3.6* below. *Table 3.3* compares the experimental and numerical eigenvectors and finds the absolute difference between them. During this portion of the experiment, the vibration of the model was particularly pronounced at the wingtips and bottom of the fuselage.

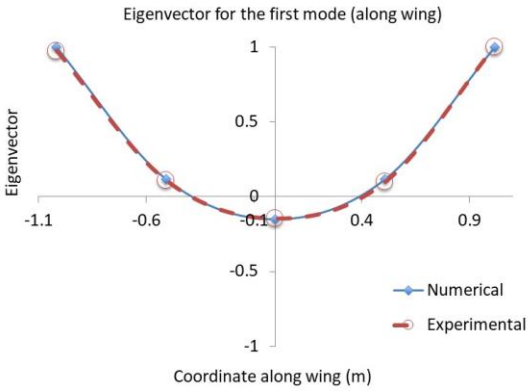

Figure 3.5 The first mode shape is symmetric along the wing

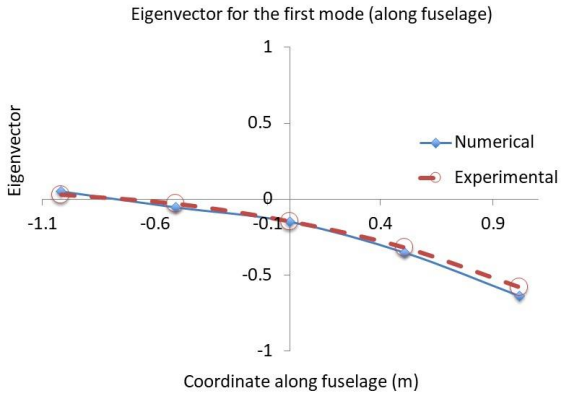

Figure 3.6 The first mode shape along the fuselage, with an increasing deviation of the plots seen in the positive x-axis

Table 3.3 The experimental and numerical eigenvectors are shown with their respective coordinates

	Fuselage Eigenvectors				
Accelerometer	1	2	3	4	5
Coordinates	-1.016	-0.508	0.00	0.508	1.016
Experiment Data	0.029	-0.031	-0.148	-0.321	-0.581
Numerical Data	0.051	-0.054	-0.150	-0.353	-0.639
Absolute Difference	0.022	0.023	0.002	0.032	0.058

	Wing Eigenvectors				
Accelerometer	6	7	3	8	9
Coordinate	-1.016	-0.508	0	0.508	1.016
Experimental Data	0.973	0.108	-0.148	0.0965	1
Numerical Data	1	0.118	-0.150	0.118	1
Absolute Difference	0.027	0.01	0.002	0.0215	0

Chapter 4

4 Discussion

4.1 Frequency response

The high quality of fit for the 3 Nyquist plots, at a minimum of 97.7%. indicates low levels of damping. Presence of damping cause a proportionate deviation of the Nyquist plot from the fitting circle. This is confirmed by the low damping ratio of 0.00631 found in Figure 3.1. Due to the limited number of data points, Microsoft Excel plotted them using arc lines. The fitting of the Nyquist plots would have been improved if more data points were taken further from the resonant frequency. With more data points close to the resonant frequency, the accuracy of ω_u and ξ would have been improved as ever closer pairs closer

While suspending the model freely reduces damping, there will always be dampening effects inherent in the system. The friction between contact surfaces of parts as well as other dissipative effects due to noise generation would have contributed to the dampening of the system. Notably, the wire used to suspend the model would have introduced friction at the nose of the fuselage. The cumulative effects of such minute dampening effects would have caused the deviation between theoretical and experimental data.

4.2 First modal shape

Examining Figure 3.5 *The first mode shape is symmetric along the wing*and Figure 3.6 *The first mode shape along the fuselage*, there is a high degree accuracy of the experimental modal shape with the numerical modal shape. Except for the right side of Figure 3.6 *The first mode shape along the fuselage*, the 2 plots align closely. As the numerical model assumes zero damping, the small absolute difference between the experimental and numerical eigenvalues can be explained by the inherent damping discussed previously. As the eigenvectors have been normalised to reflect the amount of deflection at resonance and not the actual magnitude of deflection, it can be deduced from Figure 3.5 *The first mode shape is symmetric along the wing* and that wing deflections are larger than the fuselage's. Therefore, wing deflections dominate in the first mode. Examining Table 3.3, the eigenvectors of point 6 and 9, corresponding to the tips of the wings are approximately the same. Therefore, the assumption of the model's symmetry can be assumed to be true. The small deviation would have been caused by the inherent dampening effects.

4.3 Limitations of the model idealisations

Examining Table 3.2 and the deviations from experimental values, the lumped-mass model gives a frequency closer to the experimental value. A point-mass idealisation assumes no rotational inertia and weightless bars with a suitable bending stiffness. A lumped-mass idealisation is more complex, accounting for rotational inertias that better represent an actual aircraft. The lumped mass is assumed to be spread out on one-half of the space beside them (5). However, the low difference in deviation of 0.2% does not justify the added complexity of the lumped-mass idealisation. Multiple other factors such as local temperature and the movement of the experimental setup in the workshop could have affected the actual natural frequencies (3).

Chapter 5

5 Conclusion

From this experiment, a large difference between is observed between the theoretical and experimental resonant frequency and damping ratio. This could be accounted for the by the inherent damping in the system as well as the assumptions made by the numerical models. The mode shape was predicted well as evident from the small deviation of the numerical and experimental mode shapes, for which the inherent dampening effect was responsible. The accuracy of all plots and the values of ω_u and ξ could have been improved if more data points were collected near the resonant frequency. Overall, this experiment predicts well the first undamped natural frequency and the first mode shape.

Bibliography

1. *Aerodynamic Flutter*. **Hertbert, C., et al. s.l**. : The American Institute of Aeronautics and Astronautics, Exploring Structural Dynamics.
2. Chapter 3: Real Eigenvalue Analysis. New York : University of Rochester, 3.
3. **Pinho, S.T. and Giannenas, A**. *Vibration of an aircraft model.* London : Department of Aeronautics, Imperial College London, 2018. Laboratory Handout.
4. *Fundamentals of Modal Testing.* Technologies, Agilent. Application Note 243 -3, s.l. : Agilent Technologies.
5. **Abu-Saba, E.G, Ji, Y.S and Mcginley, W.M.** *Lumped Mass Modelling For the Dynamic Analysis of Aircraft Structures.* Centre for Aerospace Research, North Carolina A & T State University, School of Engineering. North Carolina : The Journal of Aerospace Engineering, Aerospace Division, American Society of Civil Engineering.

Appendix A

Table A.1 Input frequencies and output voltages

Input		Output	
Frequency (Hz)	Frequency (rad/s)	Read Magnitude (V)	Read Phase (rad)
16.500	103.670	0.598	-3.160
16.600	104.300	0.690	-3.130
16.700	104.930	0.830	-3.100
16.800	105.560	1.020	-3.070
16.900	106.190	1.300	-3.030
17.000	106.810	1.730	-2.980
17.100	107.440	2.540	-2.890
17.200	108.070	4.650	-2.640
17.225	108.230	5.960	-2.460
17.250	108.380	7.830	-2.170
17.275	**108.540**	**9.250**	**-1.750**
17.280	**108.570**	**9.320**	**-1.660**
17.285	**108.600**	**9.330**	**-1.580**
17.290	**108.640**	**9.300**	**-1.520**
17.295	**108.670**	**9.240**	**-1.460**
17.300	108.700	9.180	-1.430
17.325	108.860	8.500	-1.170
17.350	109.010	7.820	-0.990
17.400	109.330	6.300	-0.720
17.500	109.960	4.100	-0.430

Table A.2 Acceleration data obtained during the experiment

Input	Acceleration data obtained during experiment					
Frequency (Hz)	Amplitude (V)	Load amp factor	Amplitude	Phase Angle (rad)	In-phase	Out-of-phase
16.500	0.598	0.055	10.87	-3.16	-10.87	0.20
16.600	0.690	0.055	12.55	-3.13	-12.54	-0.15
16.700	0.830	0.055	15.09	-3.10	-15.08	-0.63
16.800	1.020	0.055	18.55	-3.07	-18.50	-1.33
16.900	1.300	0.055	23.64	-3.03	-23.49	-2.63
17.000	1.730	0.055	31.45	-2.98	-31.04	-5.06
17.100	2.540	0.055	46.18	-2.89	-44.73	-11.50
17.200	4.650	0.055	84.55	-2.64	-74.13	-40.65
17.225	5.960	0.055	108.36	-2.46	-84.15	-68.27
17.250	7.830	0.055	142.36	-2.17	-80.29	-117.56
17.275	**9.250**	**0.055**	**168.18**	**-1.75**	**-29.98**	**-165.49**
17.280	**9.320**	**0.055**	**169.45**	**-1.66**	**-15.10**	**-168.78**
17.285	**9.330**	**0.055**	**169.64**	**-1.58**	**-1.56**	**-169.63**
17.290	**9.300**	**0.055**	**169.09**	**-1.52**	**8.59**	**-168.87**
17.295	**9.240**	**0.055**	**168.00**	**-1.46**	**18.58**	**-166.97**
17.300	9.180	0.055	166.91	-1.43	23.42	-165.26
17.325	8.500	0.055	154.55	-1.17	60.30	-142.30
17.350	7.820	0.055	142.18	-0.99	78.01	-118.87
17.400	6.300	0.055	114.55	-0.72	86.12	-75.53
17.500	4.100	0.055	74.55	-0.43	67.76	-31.08

Table A.3 Calculated velocity data

Input	Velocity data (calculated)			
Frequency (Hz)	Amplitude (V)	Phase Angle (rad)	In-phase	Out-of-phase
16.500	0.10	-1.59	0.00	-0.10
16.600	0.12	-1.56	0.00	-0.12
16.700	0.14	-1.53	0.01	-0.14
16.800	0.18	-1.50	0.01	-0.18
16.900	0.22	-1.46	0.02	-0.22
17.000	0.29	-1.41	0.05	-0.29
17.100	0.43	-1.32	0.11	-0.42
17.200	0.78	-1.07	0.38	-0.69
17.225	1.00	-0.89	0.63	-0.78
17.250	1.31	-0.60	1.08	-0.74
17.275	**1.55**	**-0.18**	**1.52**	**-0.28**
17.280	**1.56**	**-0.09**	**1.55**	**-0.14**
17.285	**1.56**	**-0.01**	**1.56**	**-0.01**
17.290	**1.56**	**0.05**	**1.55**	**0.08**
17.295	**1.55**	**0.11**	**1.54**	**0.17**
17.300	1.54	0.14	1.52	0.22
17.325	1.42	0.40	1.31	0.55
17.350	1.30	0.58	1.09	0.72
17.400	1.0	0.85	0.69	0.79
17.500	0.68	1.14	0.28	0.62

Table A.4 Calculated displacement data

Input	Displacement data (calculated)			
Frequency (Hz)	Amplitude (V)	Phase Angle (rad)	In-phase	Out-of-phase
16.500	0.001	-0.02	0.001	0.000
16.600	0.001	0.01	0.001	0.000
16.700	0.001	0.04	0.001	0.000
16.800	0.002	0.07	0.002	0.000
16.900	0.002	0.11	0.002	0.000
17.000	0.003	0.16	0.003	0.000
17.100	0.004	0.25	0.004	0.001
17.200	0.007	0.50	0.006	0.003
17.225	0.009	0.68	0.007	0.006
17.250	0.012	0.97	0.007	0.010
17.275	**0.014**	**1.39**	**0.003**	**0.014**
17.280	**0.014**	**1.48**	**0.001**	**0.014**
17.285	**0.014**	**1.56**	**0.000**	**0.014**
17.290	**0.014**	**1.62**	**-0.001**	**0.014**
17.295	**0.014**	**1.68**	**-0.002**	**0.014**
17.300	0.014	1.71	-0.002	0.014
17.325	0.013	1.97	-0.005	0.012
17.350	0.012	2.15	-0.007	0.010
17.400	0.010	2.42	-0.007	0.006
17.500	0.006	2.71	-0.006	0.003

Appendix B

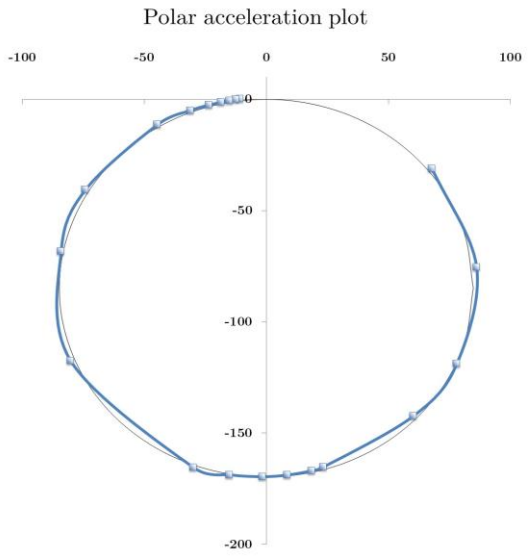

Figure B.1 Nyquist plot of acceleration. The quality of fit is 98.0%

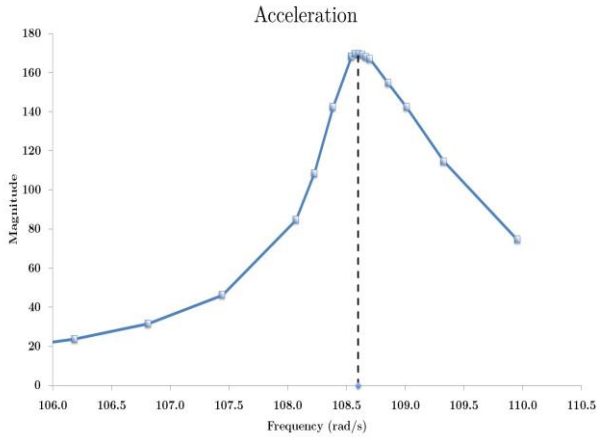

Figure B.2 The black dotted line indicates the experimental resonance frequency that corresponds to the peak acceleration magnitude

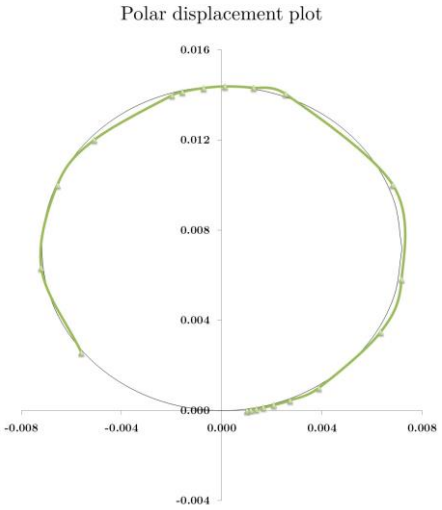

Figure B.3 Nyquist plot of displacement. The quality of fit was 97.7%

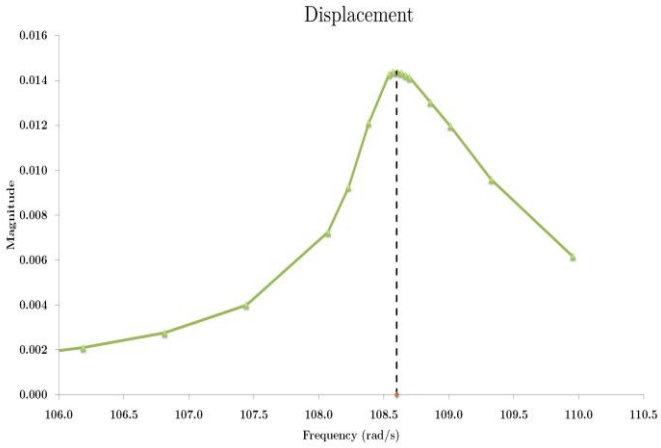

Figure B.4 The blue dotted line indicates the experimental resonance frequency that corresponds to the peak displacement magnitude